Four-port flexible UWB-MIMO antenna with triple band-notched for wearable IoT applications

Huanchen Peng, Chengzhu Du [ID] and Ruohui Wang

School of Electronics and Information Engineering, Shanghai University of Electric Power, Shanghai, People's Republic of China

Abstract

A four-port ultra-wideband (UWB) multiple-input multiple-output (MIMO) antenna with three notch bands is proposed in this work. The antenna uses ultra-thin flexible material liquid crystal polymer (LCP) as the substrate. Four identical monopole radiators are designed in this proposed antenna system. The notch bands of the antenna are generated by adding complementary split ring resonator (CSRR) and ring branch. A cross-shaped stub is set in the center of the four antenna units to enhance the isolation. The measured bandwidth of the antenna is 2.54–10.69 GHz, filtering out three notch frequency bands of 2.81–3.85, 5.11–5.98, and 7.34–8.69 GHz. The isolation in the entire working frequency is better than 22 dB. The bent performances of the MIMO system and the specific absorption rate (SAR) value are analyzed. The low SAR values, low envelope correlation coefficient (<0.05), high diversity gain (>9.999), and stable gain of the proposed antenna indicate that in UWB-MIMO systems and wearable Internet of Things applications, it can be widely used.

CAMBRIDGE
UNIVERSITY PRESS

Introduction

Ultra-wideband (UWB) technology has been a topic of heated debate since 2002, when the FCC proposed the frequency band ranging from 3.1 to 10.6 GHz for UWB applications [1]. The advantages of UWB technology are its small size, low profile, and easy manufacturing. But UWB systems may be affected by multipath fading and used frequencies ranging from 3.1 to 10.6 GHz. However, multiple-input multiple-output (MIMO) technology [2] can effectively improve system performance (such as channel capacity, multipath fading). UWB MIMO antennas with notch bands can filter out interference frequency bands, such as WiMAX (3.3–3.7 GHz), WLAN (5.15–5.35, 5.725–5.825 GHz), and X-band (7.25–7.75, 7.9–8.4 GHz). Designing an UWB-MIMO antenna which has the characteristics of multiple notches and high isolation at the same time is a difficult task.

In the past few years, many UWB MIMO antennas designed on rigid substrates are proposed [3–7], which are not suitable for wearable Internet of Things (IoT) applications. Recently, flexible UWB MIMO antennas have become more and more popular [8–13]. A two-port UWB antenna based on jeans is developed [10]. In [11], this article presents a wearable UWB toroidal four-port MIMO antenna worked at 2.4 GHz which uses silicone rubber as the substrate. A four-element single-notch MIMO antenna, of which the antenna isolation is better than 15 dB in working frequency (3.8–12 GHz), has been designed [12]. According to Du et al. [13], a flexible MIMO antenna with four ports and a single-band notch is designed, and the single-band notch is introduced by etching a C-shaped slot on the circular monopole patch.

Presented in this work is a four-port coplanar waveguide feed flexible MIMO antenna with three notch characteristics. The antenna uses a flexible ultra-thin liquid crystal polymer (LCP) material as the dielectric substrate. Four antenna units are arranged orthogonally to the isolator which is a cross-shaped stub in the center of the substrate. The measured ultra-wide bandwidth of the antenna is from 2.54 to 10.69 GHz, and three notch bands are 2.81–3.85, 5.11–5.98, and 7.34–8.69 GHz. The measured four-port isolations of the antenna are all higher than 22 dB. The flexible three band-notched MIMO antenna is suitable for wearable devices.

Antenna design

Single element antenna

In Fig. 1, the single flexible antenna is configured, which is etched on a $24 \times 30 \times 0.1$ mm^3 LCP substrate, with a dielectric constant = 2.9 and loss tangent = 0.002. This design is a slot antenna,
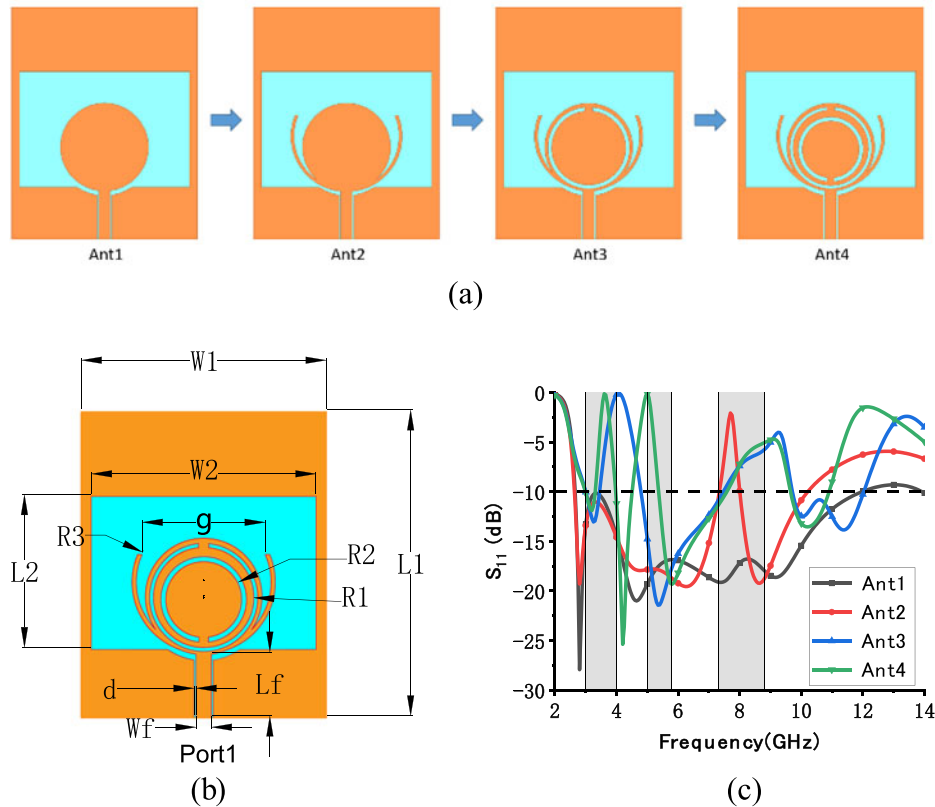
Figure 1. Single flexible UWB antenna design process: (a) structure, (b) schematic of proposed antenna, and (c) S_{11} of the single antenna.

which is composed of a circular monopole, a complementary split ring resonator (CSRR) slot, and a ring branch forming the antenna.

In this design, the total length of each CSRR slot and ring branch is set to one-half of the guide wavelength:

$$L = \frac{\lambda_g}{2} = \frac{C}{2f_{notch}\sqrt{\varepsilon_{eff}}}, \tag{1}$$

$$\varepsilon_{eff} = \frac{\varepsilon_r + 1}{2} + \frac{\varepsilon_r - 1}{2}\left(1 + \frac{12h}{w_f}\right)^{-0.5}. \tag{2}$$

In these formulas, C means the light speed, f_{notch} means the center frequency of the notch band, ε_r represents the relative dielectric constant of the proposed substrate, and ε_{eff} represents the effective value of the dielectric constant.

After optimization in HFSS, the optimal parameter values in Fig. 1(b) are as follows: L1 = 30 mm, L2 = 15 mm, Lf = 6.25 mm, g = 1.35 mm, Wf = 1.5 mm, W1 = 24 mm, W2 = 22 mm, d = 0.2 mm, R1 = 4.6 mm, R2 = 3.7 mm, and R3 = 6.6 mm.

Figure 1(c) plots S-parameters for the above antennas. The Ant1 is a circular monopole antenna, which the impedance bandwidth is 2.65–11.97 GHz. Then, by adding a ring branch on the Ant1, the Ant2 has the first notch band at 7.5 GHz. Finally, by loading the outer and inner rings of the CSRR on the Ant2, respectively, the Ant3 has another notch band at 3.5 GHz, and the Ant4 has the last notch band at 5.25 GHz (Figure 2).

Four-element MIMO antenna

Figure 3(a) illustrates the structure of the entire system which is etched on a $65 \times 65 \times 0.1$ mm^3 LCP substrate. To increase isolation between four antenna units, a cross-shaped stub is placed in the middle, and the grounds of four units are not connected.

The parameter values depicted in Fig. 3(a) are as follows: d1 = 1 mm, L3 = 59.3 mm, L = 65 mm, W = 65 mm, α = 9°. The angle β between the cross-shaped stub is 91 degrees.

Decoupling structure design process

Decoupling structure design process is shown in Fig. 4. For simplicity, only S11, S21, and S31 are studied since they are symmetrically arranged. In Fig. 4(a), four units are placed orthogonally with each other without any isolation in Ant5. Ant6 is the evolution of Ant5 with one cross-shaped stub in the center of the substrate. Ant7 has two paralleled cross-shaped stubs in the middle of the substrate. And, Ant8 has three paralleled cross-shaped stubs in the middle of the substrate.

Through Fig. 4(b), it is clear that after adding the cross-shaped stub, the antenna can still cover the working frequency ranging from 2.58 to 11.32 GHz. But the second notch band in Ant5 and Ant6 is lower than others. To achieve a better notch band and a wider impedance bandwidth, the number of cross-shaped stubs is increased.

As depicted in Fig. 4(c) and (d), whether with or without the cross-shaped stub structure, the frequency range of S21 less than −20 dB is almost unchanged. However, the change of S31 is obvious. After loading the cross-shaped stub, especially with three
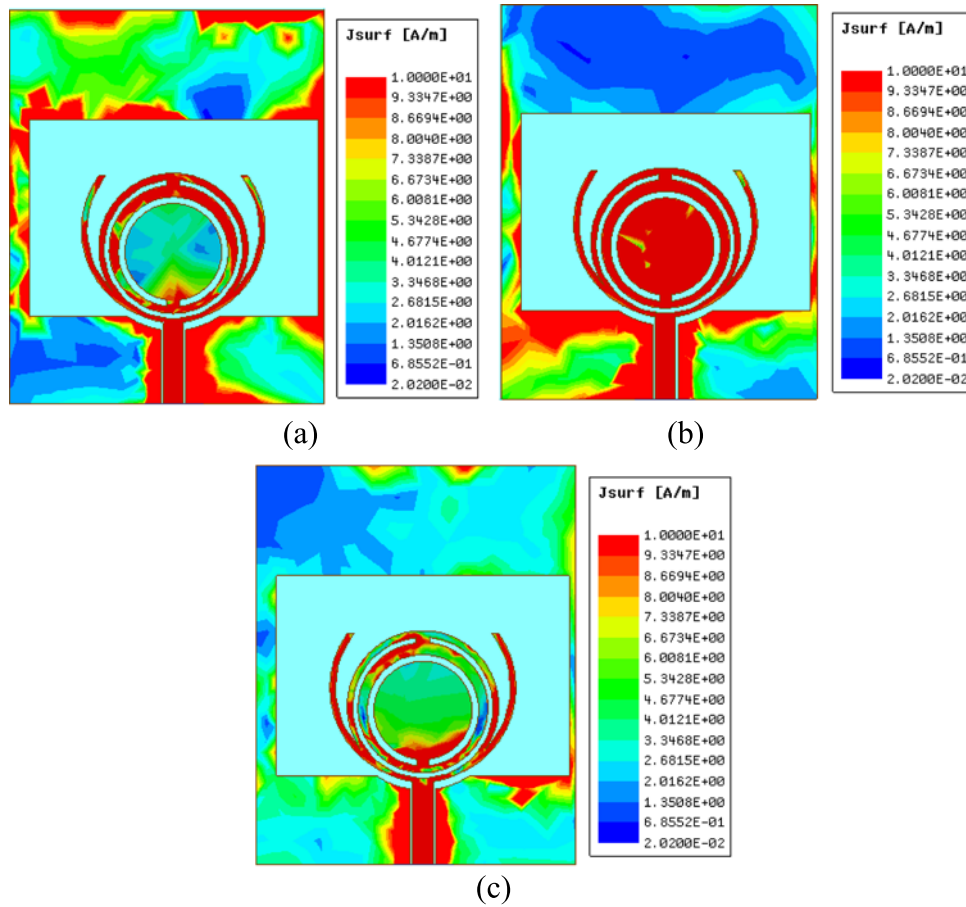
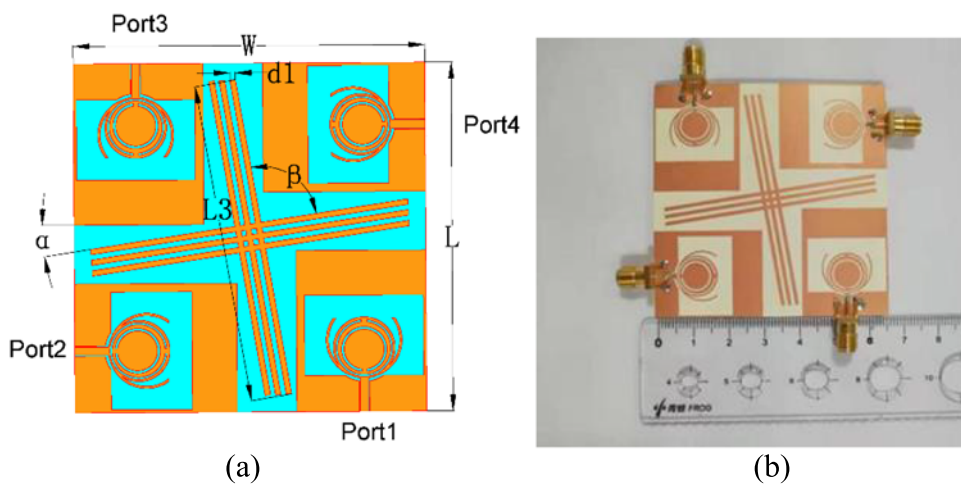**Figure 2.** Distributions of surface current at: (a) 3.5 GHz, (b) 5.25 GHz, and (c) 7.5 GHz.

Figure 3. Four-element antenna: (a) schematic and (b) manufactured antenna.

paralleled stubs, the value of S31 in the low frequency part has dropped from about −15 dB to below −20 dB. The cross-shaped stub acts as a reflector to effectively improve the isolation and reduce electromagnetic coupling between four ports, especially the diagonal units.

Envelope correlation coefficient (ECC) generally characterizes the relationship between two elements, so MIMO systems will use multiple sets of ECC to characterize the independence between antennas. In Fig. 4(e), it can be easily found that all values of ECC are lower than 0.1 and the ECC in Ant8 is better than others. As a result, three paralleled cross-shaped stubs are chosen for better antenna performance.

Figure 5 shows the surface current distribution with/without the cross-shaped stub at 5.5 GHz. From Fig. 5(a), it can be seen
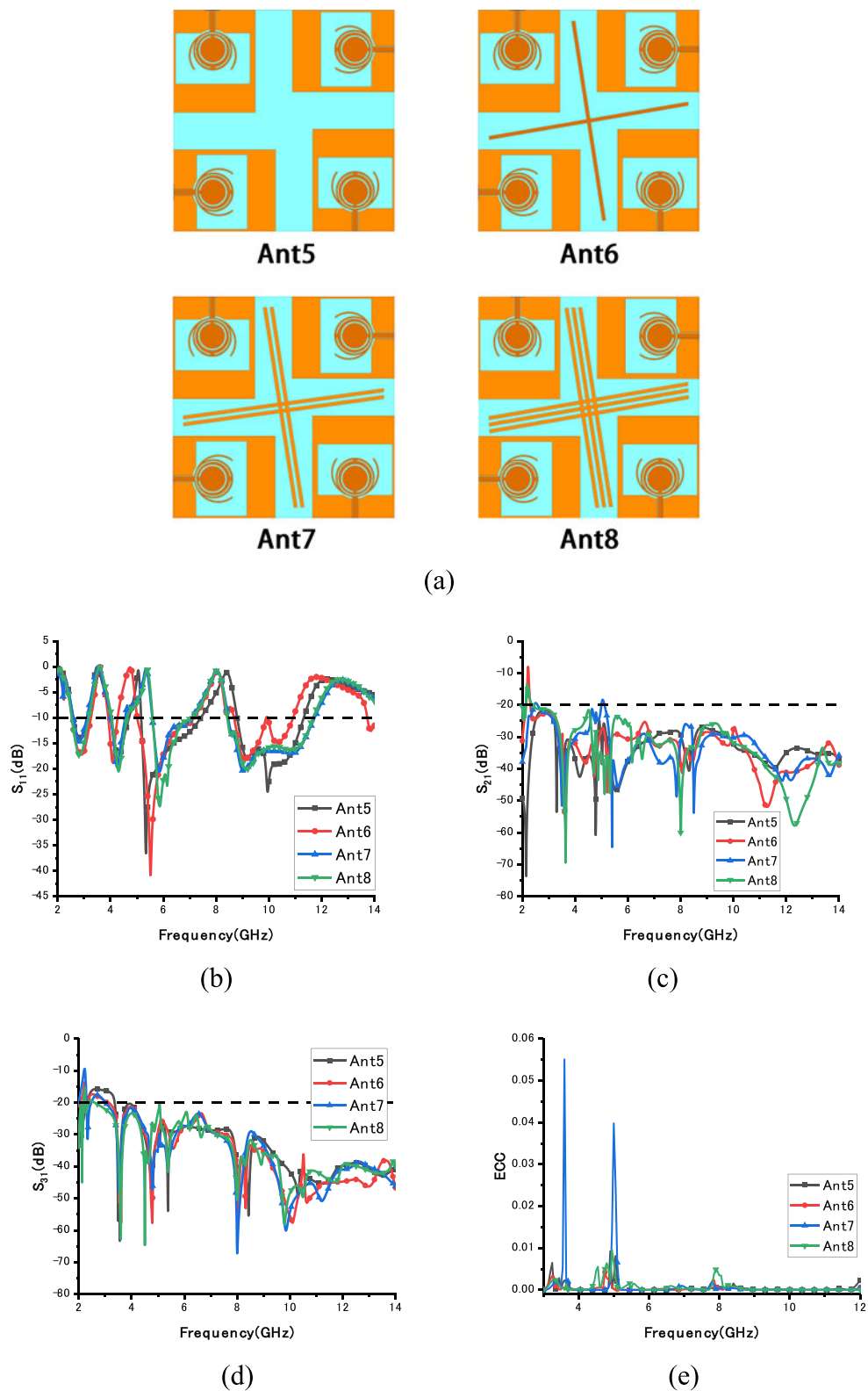
Figure 4. Comparison of four-element antenna: (a) evolution of four-element antenna, (b) S11, (c) S21, (d) S31, and (e) ECC.

that in the absence of the cross-shaped stub, a large amount of current is coupled to the other ports. In contrast, in Fig. 5(b), when a cross-shaped stub is used, most of the current stops flowing to other ports, and the port isolation is greatly improved.

MIMO antenna with connected ground

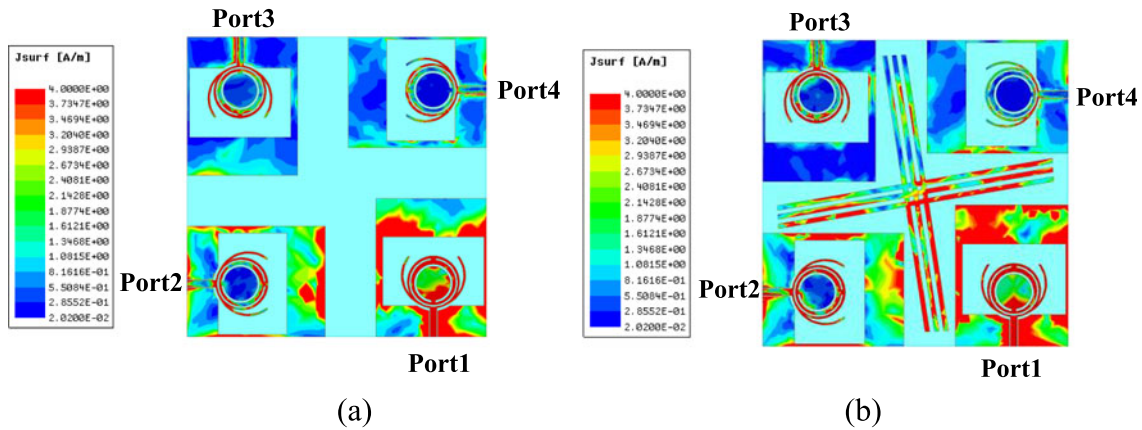Four-port MIMO antenna with connected ground is also designed and analyzed.

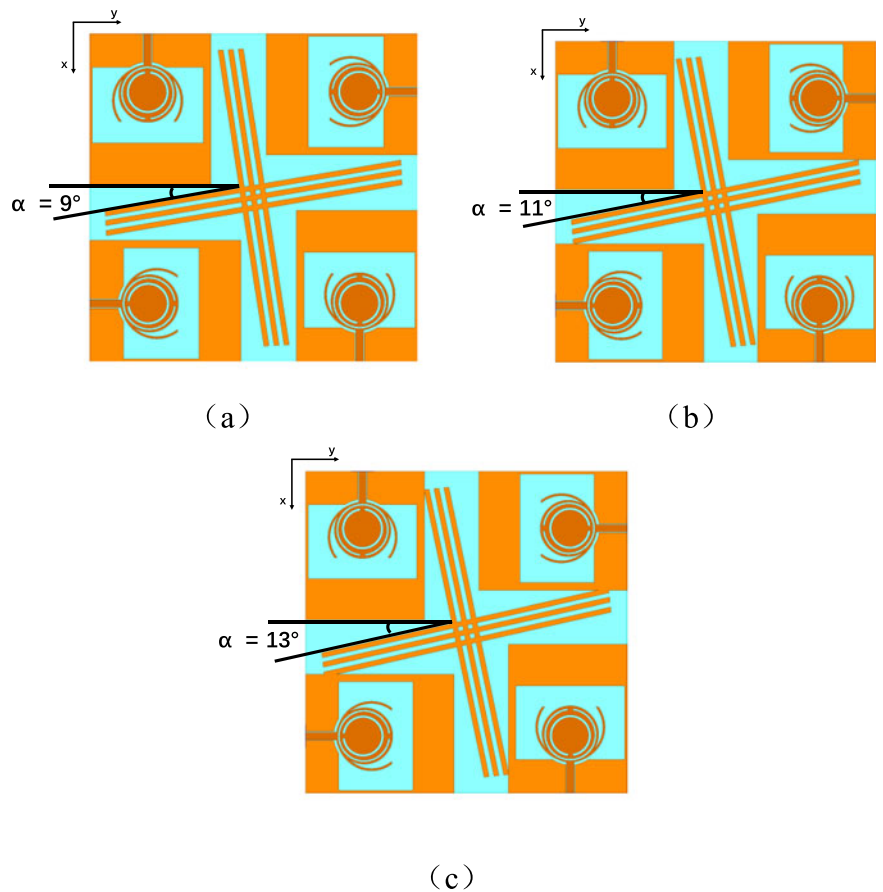**Figure 5.** Surface current distributions: (a) without stub and (b) with stub.

Figure 6. Different relative positions between decoupling structures and antenna: (a) $\alpha = 9°$, (b) $\alpha = 11°$, and (c) $\alpha = 13°$.

In Fig. 6(c), when the isolation structure is connected to four units, the simulated bandwidth of the antenna is 2.45–10.68 GHz, filtering out three notch frequency bands of 3.06–3.98, 4.51–5.28, and 7.39–8.59 GHz, which can still filter WiMAX signals at 3.5 GHz, WLAN signals at 5.25 GHz and X-band signals at 7.5 GHz. The isolation in the entire working frequency is better than 15 dB.

Due to the fact that the angle β between the cross-shaped stub is 91 degrees, when the decoupling structure is rotated centered around the midpoint of the substrate, three situations occur in Fig. 6. When the parameter α is 9 degrees, the isolation stubs are not connected with four elements. And when the parameter α is 11 degrees, the isolation stubs are connected with two diagonal elements. Finally, when the parameter α is 13 degrees, the isolation stubs are connected with four elements, respectively.

The influence of different α on S11, S21, and S31 is plotted in Fig. 7, adjusting α from 9 to 13 degrees. From Fig. 7(a), as α increasing, the impedance bandwidth of the antenna becomes narrow, and the second notch band shifts to the left slightly. From Fig. 7(b), when the frequency is from 2.3 to 3.3 GHz, S21 is slightly fluctuating around −20 dB and the isolation in the other band is all below −20 dB. It can be found in Fig. 7(c) that different relative positions have little influence on S31.
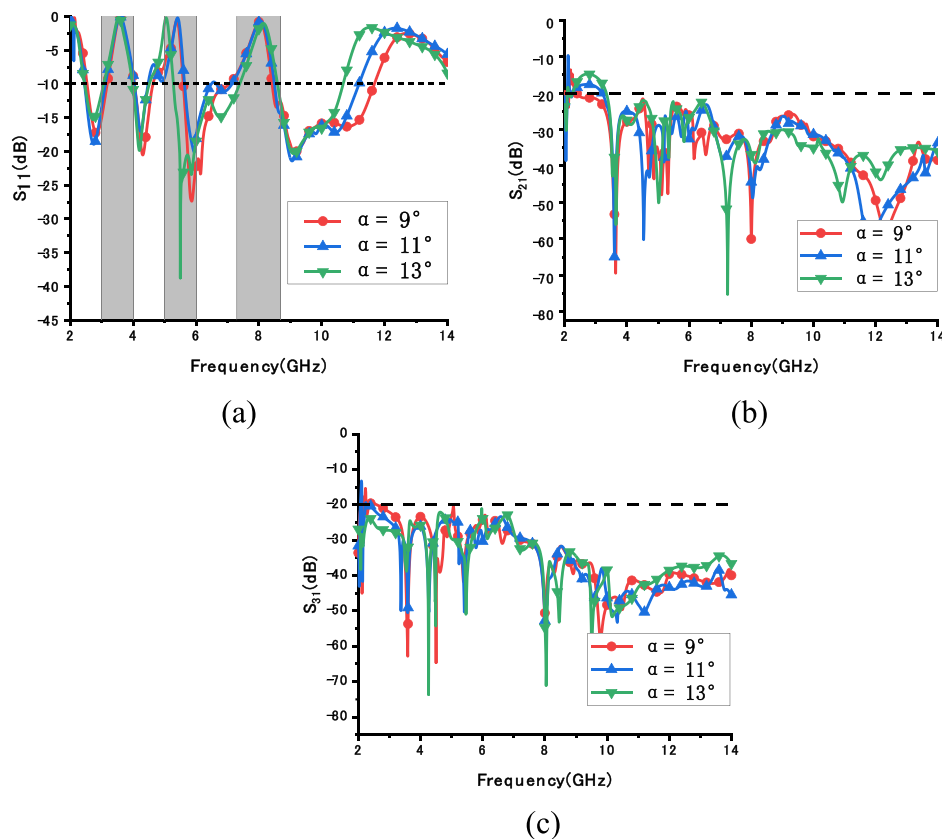
Figure 7. Different S-parameters when α equals to different values: (a) S11, (b) S21, and (c) S31.

Experimental verification

S-parameter

MIMO antenna without connected ground was finally fabricated. S-parameters were measured using an Agilent E8362B network analyzer. Port 1 is excited during the measurement, while the rest ports are connected to 50-ohm loads. It can be seen in Fig. 8(a) that the measured return loss of that antenna is 2.54–10.69 GHz, except for the three frequency bands that fall between 2.54 and 10.69 GHz, namely 2.81–3.85, 5.11–5.98, and 7.34–8.69 GHz. As a result, the antenna can filter WiMAX signals at 3.5 GHz, WLAN signals at 5.5 GHz, and X-band signals at 8.1 GHz. According to Fig. 8(b), it is clear that the measured parameters are better than the simulated ones. In the entire band, measured S21 and S31 are all less than −22 dB.

To clarify the bending characteristics of the MIMO antenna, the entire design was bent both along the E-plane and H-plane, with bending radii of 30 and 45 mm, respectively. When port 1 is excited, the E-plane and H-plane is shown in Fig. 8(c). From Fig. 8(d) and (e), it is obvious that the antenna's S-parameters are influenced by bending conditions. Bending along the E-plane has a greater impact on the antenna's return loss than along the H-plane. Bending along the E-plane, the isolations are all better than 24 dB. Bending along the H-plane, the isolations are all better than 21 dB. As a result, under bending conditions, this MIMO system exhibits good performances.

In Fig. 8(f), the S-parameters are measured when the antenna is set on the human body. When the processed antenna system is attached to different parts of human body, such as the arm, thigh, and chest, respectively, the S-parameters are measured. As a result,

the measured notch bands become narrow, especially at the high frequency band. But WiMAX, WLAN, and X-band notch bands still remain covered. The isolations of the antenna are all better than 30 dB.

Radiation patterns

Three frequency points of 4.5, 6, and 9.3 GHz are selected as the test frequency points of the normalized far-field radiation pattern of the antenna. In Fig. 9, each figure contains the simulated and measured radiation patterns of the co-planar polarization and cross polarization of the E-plane and the H-plane. It can be observed from the figure that the proposed antenna has good radiation performance, except for some deteriorations in the high-frequency state due to imperfect testing environment, but this does not affect the ability of the antenna to receive and transmit signals.

Gain and diversity performance

It can be seen from the Fig. 10(a) that in the UWB range, except for the three stop bands, the gain changes gently, and the measured gain varies between 3.6 and 6.87 dB.

To assess the correlation between MIMO antenna channels, ECC and diversity gain (DG) can be introduced. In general, the calculated ECC values are more accurate by equation (3) based on far-field radiation [14] than equation (4) with S-parameters [15], and the DG can be estimated by equation (5) [16]. Figure 10(b) indicates that the ECC value in the UWB frequency band is less than 0.05 except for the three stopbands. The DG curve in Fig. 10(c) shows that DG is greater than 9.999 except for the three stopbands
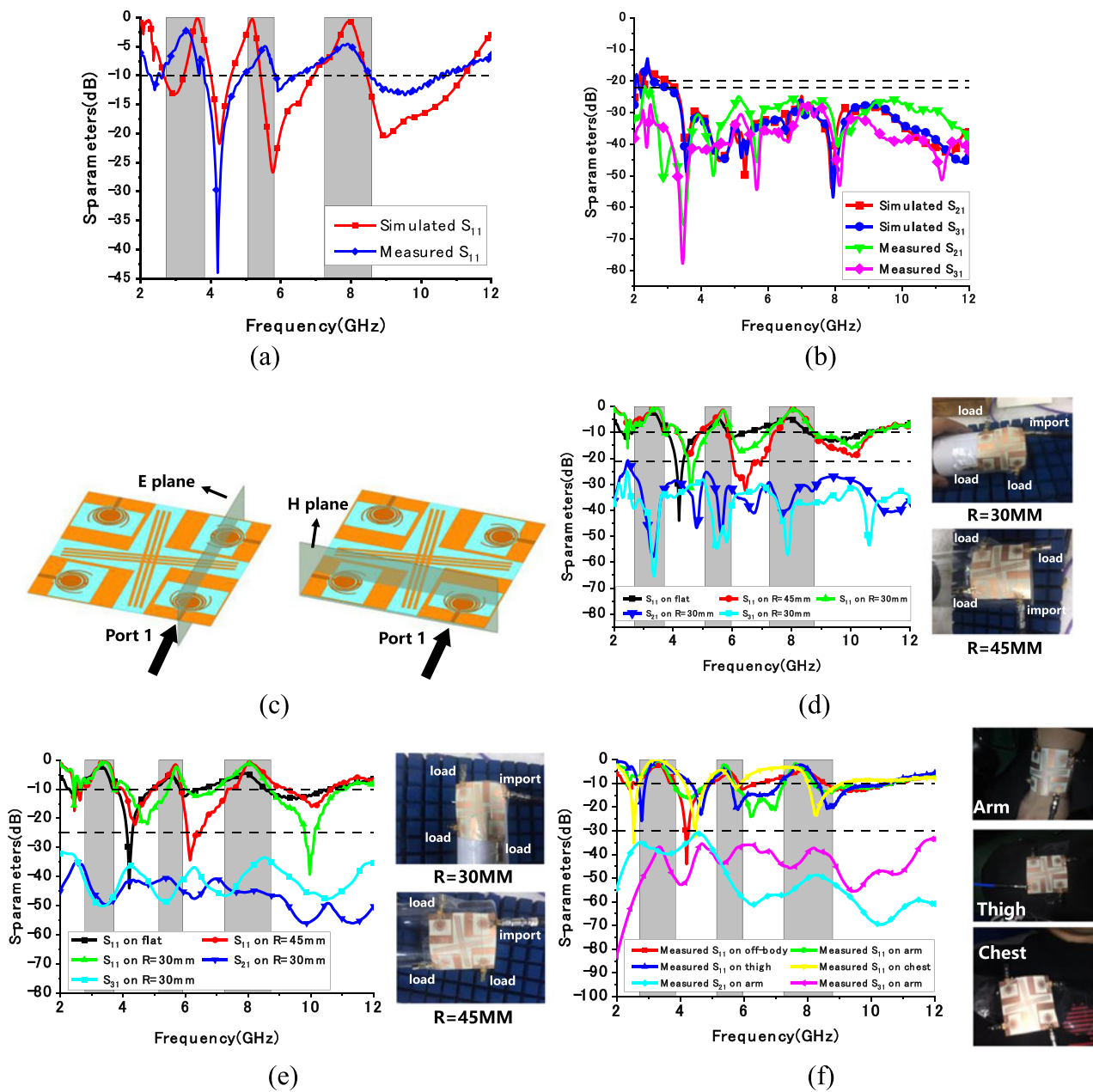
Figure 8. Antenna measured and simulated results. (a) S11 of simulation and measurement, (b) isolation of simulation and measurement, (c) when Port 1 is excited, the location of E-plane and H-plane, (d) measured S-parameters of antenna, respectively, bent along different radius *R* at E-plane, (e) measured S-parameters of antenna, respectively, bent along different radius *R* at H-plane, and (f) S-parameters when antenna is on human body.

in the operating frequency band. It is evident from all of the above that the proposed antenna has good independence.
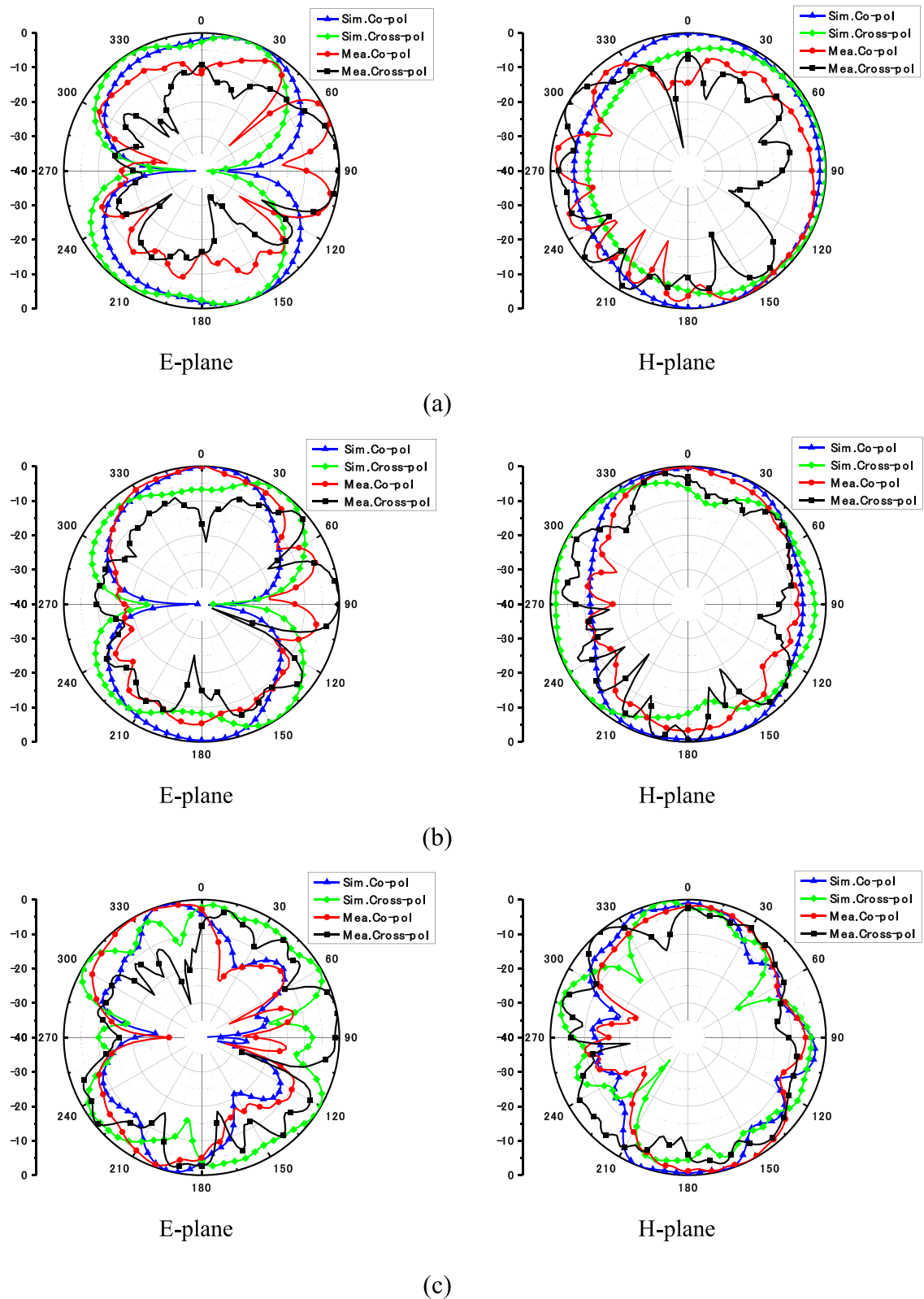
$$\rho_e\left(i, j, N\right) = \left| \frac{\sum_{n=1}^{N} S_{i,n}^* S_{n,j}}{\left| \prod_{k=i,j} \left(1 - \sum_{n=1}^{N} S_{k,n}^* S_{n,k}\right) \right|^{\frac{1}{2}}} \right|^2, \quad (3)$$

$$\rho_e\left(i, j\right) = \frac{\left| \iint_{4\pi} \vec{F}_i\left(\theta, \varphi\right) \cdot \vec{F}_j\left(\theta, \varphi\right) d\Omega \right|^2}{\iint_{4\pi} \left| \vec{F}_i\left(\theta, \varphi\right) \right|^2 d\Omega \cdot \iint_{4\pi} \left| \vec{F}_j\left(\theta, \varphi\right) \right|^2 d\Omega} \quad (4)$$

$$DG = 10\sqrt{1 - (ECC)^2}. \quad (5)$$

The total active reflection coefficient (TARC) is introduced to reflect the behavior of the MIMO antenna, which can reflect the coupling of the MIMO system. For a four-element antenna system, its calculation formula is as follows [17]:

$$TARC = N^{-0.5} \sqrt{\sum_{N}^{i=1} \left| \sum_{N}^{k=1} S_{ik} e^{j\theta_{k-1}} \right|^2}, \quad (6)$$

Figure 9. Simulated and measured radiation patterns: (a) 4.5, (b) 6, and (c) 9.3 GHz.

where N is the number of antenna and denotes the phase angle of the excitation source input by the antenna. Figure 11 shows the simulated and measured TARC curves of the antenna when $\alpha = 0°$, 60°, 120°, and 180°, respectively. It can be observed that

the simulated TARC is similar to the simulated return loss, and the measured TARC is similar to the measured return loss. It shows that the coupling effect of the antenna is low and the radiation efficiency of the antenna is relatively high.
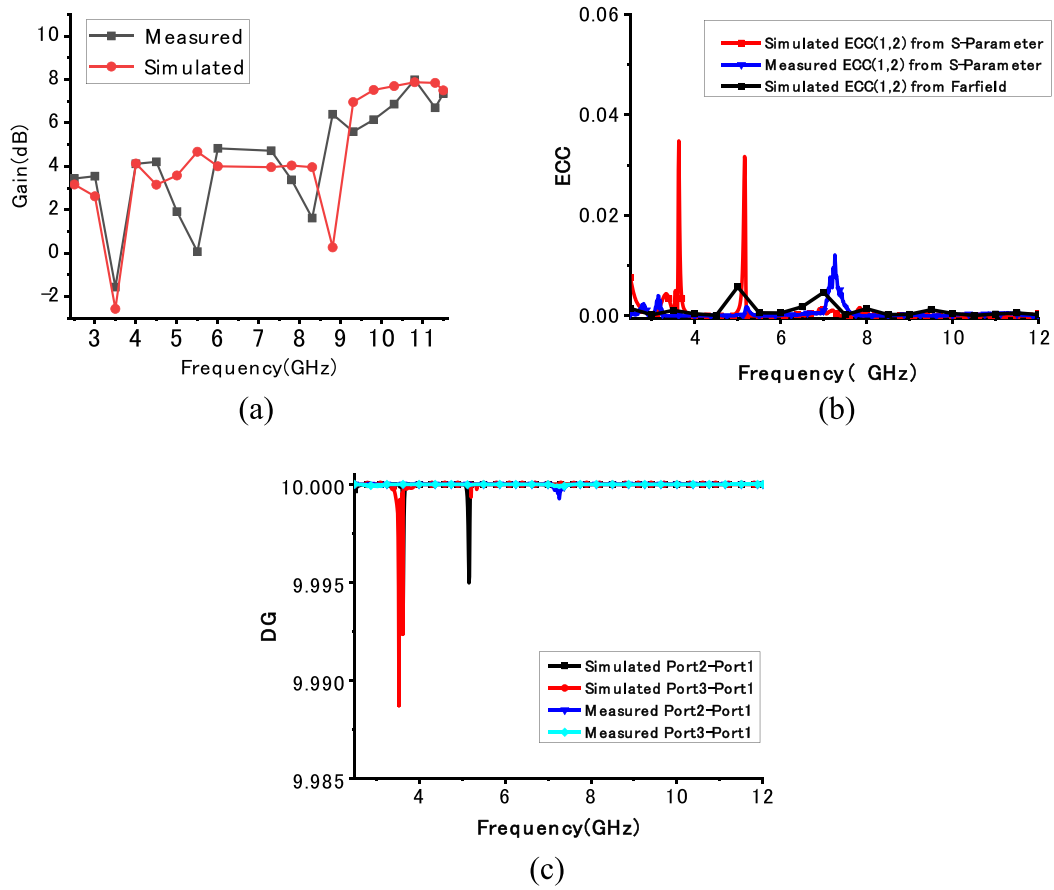
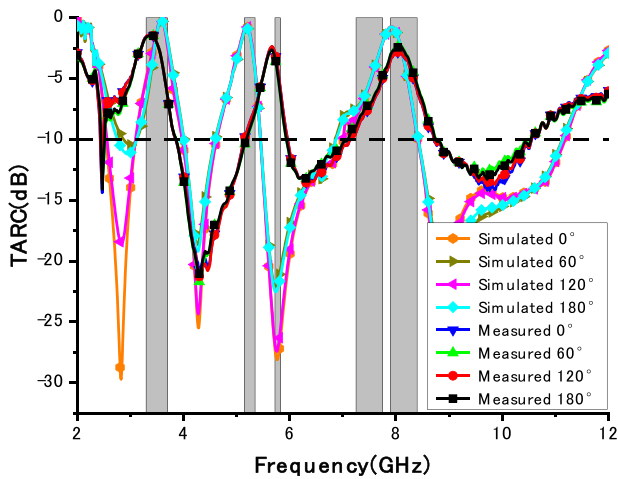**Figure 10.** Measured and simulated results: (a) gain, (b) ECC, and (c) DG.

Figure 11. Simulated and measured TARC of the proposed antenna.

Table 1. Maximum SAR values on various conditions

Frequency	4.2 GHz	6 GHz	9.2 GHz
10 g Tissue (W/kg) (H1 = 3 mm)	0.3079	0.4842	0.2345
10 g Tissue (W/kg) (H1 = 3 mm)	0.1381	0.4013	0.2056

SAR

The specific absorption rate (SAR) represents the sum of electromagnetic radiation absorbed by human tissue in a given time
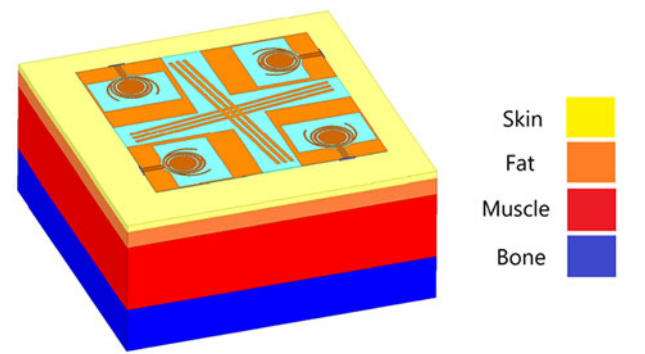
Figure 12. Model of human body tissue.

Table 2. The parameters of human body tissue

	Bone	Muscle	Fat	Skin
ε_r	18.49	52.67	5.27	37.95
σ (S/m)	0.82	1.77	0.11	1.45
Density (kg/m^3)	1008	1006	900	1001
Thickness (mm)	13	20	5	2

period [18]. The simulated SAR of the antenna is calculated by HFSS 18.0 software. The structure of the simulated human tissue model is depicted in Fig. 12. The total size of the model is 75 mm × 75 mm × 40 mm. The distance between the antenna

Table 3. Comparison of the designed antenna with other reported antennas

Ref.	Polarization	No. of ports and size (mm^3)	Bandwidth (GHz)	Feeder method	Substrate (dielectric constant)	Notch band bandwidth (GHz)	Peak gain (dB)	Iso. (dB)
[4]	Linear	4, 80*80*1.6	2.1–20	CPW	FR4 (4.4)	3.3–4.1, 8.2–8.6	5.8	25
[5]	Linear	4, 45*45*0.508	3–14	Microstrip	GML 1000 (3.2)	5.15–5.35, 7.25–7.745	4.7	20
[6]	Linear	4, 36*36*0.762	3–10.6	Microstrip	Neltec (3.2)	3.28–4.3, 4.9–5.5	5	20
[7]	Linear	4, 39*39*1.6	2.30–13.75	Microstrip	FR4 (4.4)	3.25–3.75, 5.08–5.90, 7.06–7.95	4.6	22
[11]	Linear	4, 40*12*2	3.1–12	Microstrip	Silicone Rubber (2.9)	0	3.1	20
[12]	Linear	4, 40*40*0.145	3.8–12	CPW	PET File (2.8)	4.9–6	5	15
[13]	Linear	4, 65*65*0.1	2.85–10.85	CPW	LCP (2.9)	4.9–6.425	11	24
[15]	Linear	4, 65*65*0.1	2.9–10.86	CPW	LCP (2.9)	0	6.49	17
Prop.	Linear	4, 65*65*0.1	2.54–10.69	CPW	LCP (2.9)	2.81–3.85, 5.11–5.98, 7.34–8.69	6.87	22

system and the human body model is H1. The input power is 0.1 w, the variables H1 = 3 mm and 5 mm, and the simulated SAR values at 4.2, 6, and 9.2 GHz are shown in Table 1. It can be found from Table 1 that the simulated SAR values are far lower than the EU standard of 2 W/kg/10 g organization, which shows that the radiation energy of the antenna has a particularly small impact on human tissues (Table 2).

Performance comparison

Based on the substrate material, number of ports, bandwidth, feeder method, notch band, peak gain, and isolation, the designed antenna in this article is compared with other published antennas in Table 3. It can be seen that [4–7] are all UWB MIMO antennas with notch bands, but they are all etched on rigid substrates. Although flexible MIMO antennas are designed in [11–13, 15], they have less than two notch bands. However, the proposed antenna adds more notch bands, while ensuring broad band. The antenna in this article is composed of flexible material, three notch bands, four ports, CPW feed, stable gain, and higher isolation. Therefore, the proposed antenna has many good performances for flexible device.

Conclusion

This article shows a new flexible four-element UWB MIMO antenna with triple notch-band characteristics which uses LCP as the substrate. The reject bands of 2.81–3.85, 5.11–5.98, and 7.34–8.69 GHz are generated by engraving the CSRR groove on each radiator and loading the ring branch. In the whole band, the isolation is higher than 22 dB due to the cross-shaped stubs inserted between each of the four elements. Furthermore, the

antenna performs well in bent states. The low SAR values, lower ECC (<0.05), good DG (>9.999), and stable gain indicate that the antenna is suitable for UWB-MIMO systems and wearable IoT applications.

References

1. **Li R and Zhu L** (2007) Compact UWB bandpass filter using stub-loaded multiple-mode resonator. *IEEE Microwave and Wireless Components Letters* **17**(1), 40–42.
2. **Kaiser T, Zheng F and Dimitrov E** (2009) An overview of ultra-wide-band systems with MIMO. *Proceedings of the IEEE* **97**(2), 285–312.
3. **Jayant S and Srivastava G** (2020) Four elements UWB MIMO antenna array. In *2020 7th International Conference on Signal Processing and Integrated Networks (SPIN)*. IEEE, 48–54.
4. **Rekha SD, Pardhasaradhi P, Madhav BTP and Devi YU** (2020) Dual band notched orthogonal 4-element MIMO antenna with isolation for UWB applications. *IEEE Access* **8**, 145871–145880.

5. **Muzaffar K and Magray MI** (2019) Compact four element dual band notched orthogonally placed UWB antennas for wireless MIMO applications. In *2019 IEEE-APS Topical Conference on Antennas and Propagation in Wireless Communications (APWC)*. IEEE.

6. **Sipal D, Abegaonkar MP and Koul SK** (2018) Compact planar four element dual band-notched UWB MIMO antenna for personal area network applications. In *12th European Conference on Antennas and Propagation (EuCAP 2018)*.

7. **Tang Z, Wu X, Zhan J, Hu S, Xi Z and Liu Y** (2019) Compact UWB-MIMO antenna with high isolation and triple band-notched characteristics. In *IEEE Access*, 1–1.

8. **Dey AB, Pattanayak SS, Mitra D and Arif W** (2021) Investigation and design of enhanced decoupled UWB MIMO antenna for wearable applications. *Microwave and Optical Technology Letters* **63**(3), 845–861.

9. **Li W, Hei Y, Grubb PM, Shi X and Chen RT** (2018) Compact inkjet-printed flexible MIMO antenna for UWB applications. *IEEE Access* **6**, 50290–50298.

10. **Biswas AK and Chakraborty U** (2019) Investigation on decoupling of wide band wearable multiple-input multiple-output antenna elements using microstrip neutralization line. *International Journal of RF and Microwave Computer-Aided Engineering* **29**, e21723.

11. **Govindan T, Palaniswamy SK, Kanagasabai M, Kumar S, Rama Rao T and Alsath MGN** (2021) Conformal quad-port UWB MIMO antenna for body-worn applications. *International Journal of Antennas and Propagation* **2021**, 1–13.

12. **Sethi WT, Issa K and Alshebeili SA** (2019) An inkjet-printed UWB-MIMO antenna with band rejection capability for wireless network applications. In *2019 2nd International Conference on Computer Applications & Information Security (ICCAIS)*. IEEE, 1–5.

13. **Du C, Yang Z and Zhong S** (2022) A compact coplanar waveguide-fed band-notched four-port flexible ultra-wide band-multi-input-multi-output slot antenna for wireless body area network and Internet of Things applications. *International Journal of RF and Microwave Computer-Aided Engineering* **32**(9), e23289.

14. **Blanch Boris S, Romeu Robert J and Corbella Sanahuja I** (2003) Exact representation of antenna system diversity performance from input parameter description. *Electronics Letters* **39**(9), 705–707.

15. **Zhang J, Du C and Wang R** (2022) Design of a four-port flexible UWB-MIMO antenna with high isolation for wearable and IoT applications. *Micromachines* **13**(12), 2141.

16. **Tian R, Lau BK and Ying Z** (2011) Multiplexing efficiency of MIMO antennas. *IEEE Antennas and Wireless Propagation Letters* **10**, 183–186.

17. **Pandit S, Mohan A and Ray P** (2018) A compact four element MIMO antenna for WLAN applications. *Microwave & Optical Technology Letters* **60**(2), 289–295.

18. **Pei LR, Du C, Shi CX and Peng HC** (2022) A gain enhanced low SAR dual-band MIMO antenna integrated with AMC for wearable ISM applications. In *2022 7th International Conference on Communication, Image and Signal Processing (CCISP)*. IEEE, 371–375.

Huanchen Peng was born in Shanghai, China in 1999. He received the B.S. degree from the Shanghai University of Electric Power in 2021. He is currently pursuing the M.S. degree in College of Electronics and Information Engineering, Shanghai University of Electric Power. His research interests include Circular polarization antenna, flexible antenna and multiband MIMO antenna.

Chengzhu Du was born in Haikou, Hainan Province, China. She received the B.S. degree from the Xidian University, M.S. degree from Nanjing University of Posts and Telecommunications, and PhD degree from Shanghai University, in 1995, 2003, and 2012, respectively, all in electromagnetic wave and microwave technology. She is currently an associate professor of Shanghai University of Electric Power. Her research interests include flexible antenna and textile antenna, multiband and wideband antennas, and MIMO technologies.

Ruohui Wang was born in Xinxiang, Henan Province, China in 1998. She received the B.S. degree from the Shanghai University of Electric Power in 2020. She is currently pursuing the M.S. degree in College of Electronics and Information Engineering, Shanghai University of Electric Power. Her research interests include UWB-MIMO antenna, flexible antenna, and Millimeter-wave antenna.